

Measuring Aerosol Active Surface Area by Direct Ultraviolet Photoionization and Charge Capture in Continuous Flow

R.T. Nishida^a, T.J. Johnson^a, A.M. Boies^{a,b}, and S. Hochgreb^a

^aDepartment of Engineering, University of Cambridge, Cambridge CB2 1PZ, UK

^bDepartment of Civil, Environmental and Geo-Engineering, University of Minnesota, Minneapolis, Minnesota 55455

August 22, 2019

Abstract

Direct ultraviolet photoionization electrically charges particles using a mechanism distinct from diffusion charging. The purpose of this study is to evaluate aerosol photoemission theory as a function of aerosol particle size, concentration, material, and morphology. Particles are classified using an aerodynamic aerosol classifier (AAC) and subsequently measured with a scanning mobility particle sizer (SMPS) and photoionization measurement system in parallel. This configuration allows direct comparison of photo-emission from high concentrations of initially neutral, monodisperse aerosols with different morphologies or materials. Under all examined conditions, the overall photoelectric yields of particles of self-similar material (silver and unconditioned soot) and morphology (sintered spheres and agglomerates) are each linearly proportional to the second moment of the mobility-equivalent diameter distribution, even in the transition regime (mobility diameter 30 - 200 nm), with agglomerate silver particles resulting in $5\times$ higher photoelectric yield than unconditioned soot from a propane flame. It is shown for the first time that the photoelectric yield is significantly higher ($2.6\times$) for fractal-like agglomerate silver particles than sintered, close-packed spherical particles of the same material and mobility-equivalent diameter, which is inferred to be due to the larger material surface area exposed externally to the particle surroundings. It is demonstrated that photoelectric measurements of aerosols reflect the photoelectrically active surface area which depends on the particle morphology and therefore the state of sintering.

Corresponding author: R.T. Nishida

Email address: rn359@alumni.cam.ac.uk

Running Title: Aerosol Active Surface Area by Photoionization

Nomenclature

Roman Symbols

A	area concentration, $\text{nm}^2 \text{cm}^{-3}$
c	operation constant
d	particle diameter, nm
D_{fm}	mass-mobility exponent
e	electron charge, $1.602 \times 10^{-19} \text{ C}$
h	Planck's constant, $6.626068 \times 10^{-34} \text{ kg m}^2 \text{ s}^{-1}$
$h\nu$	photon energy, eV
I	radiative energy flux, W m^{-2}
i	current, A
K_c	photoemission constant, J^{-2}
k_m	prefactor
m	mass, kg; empirically determined constant
N	particle number concentration, cm^{-3}
n	number of primary particles
$p(d)$	probability density function
Q	volumetric flow rate, std L/min
q	particle charge level
S	shape factor
t	time, s
ν	photon frequency, s^{-1}
Y	quantum yield per incident photon

Greek Symbols

$\alpha^{q \rightarrow q+1}$	combination coefficient for photoionisation, s^{-1}
Φ	work function, eV
ρ	density, kg m^{-3}
σ_{ph}	photoelectrically active surface area, nm^2

Subscripts

2	second moment average
ae	aerodynamic equivalent
cl	close packed
e	electrode; exposed
eff	effective
irr	irradiation
m	mobility
o	outlet
p	particle
ph	photoelectric
pp	primary particle
q	charge level index
s	charge saturation; surface
ε	photoelectric activity
ve	volume equivalent

Acronyms / Abbreviations

AAC	Aerodynamic Aerosol Classifier
CMD	Count Median Diameter
CPC	Condensation Particle Counter

DC Diffusion Charging; Direct Current
DMA Differential Mobility Analyzer
DOS Di-Octyl Sebacate
HEPA High Efficiency Particulate Air
PAH Polycyclic Aromatic Hydrocarbon
PC Photoelectric Charging
SMPS Scanning Mobility Particle Size Spectrometer
UV Ultraviolet

1 Introduction

Direct ultraviolet (UV) photoionization is a method for electrically charging aerosols which enables measurements distinct to those from diffusion charging. Direct UV photoionization can yield higher electrical charge states than diffusion charging methods for some nanoparticle materials (Jung and Kittelson, 2005; Jung et al., 1988; Li and Chen, 2011; Matter et al., 1995; Mohr et al., 1996) and the process is material and surface-dependent (Burtscher et al., 1982, 1984; Burtscher, 1992; Burtscher et al., 1998; Jung and Kittelson, 2005; Keller et al., 2001; Matter et al., 1995; Mohr et al., 1996; Niessner, 1986; Ott and Siegmann, 2006; Matter et al., 1999; Bukowiecki et al., 2002; Kittelson et al., 2005; Burtscher, 2005). The dependence on particle material and increased charging efficiency, particularly at low particle sizes ($d_p < 50$ nm), is of interest for emissions measurement (Jung and Kittelson, 2005), particle classification (Hontañón and Kruis, 2008), capture (Jiang et al., 2007b; Kulkarni et al., 2002; Hogan et al., 2004), controlled deposition (Byeon and Roberts, 2014), and fundamental studies of nanoparticle material and surface properties (Burtscher et al., 1982; Weber et al., 2001, 1999; Röhrbein and Weber, 2018).

The dependence of photoelectric yield on material or surface properties introduces the opportunity for sensing aerosol material type when particle size and concentration information is known. For example, it has been demonstrated that by combining material-dependent (photoemission) and material-independent (unipolar diffusion charging) measurements adjusted for particle size and concentration, a chemical fingerprint of the surface properties of an aerosol may be determined (Burtscher, 1992; Keller et al., 2001). The photocharging (PC) to diffusion charging (DC) ratio was used to investigate a range of indoor and outdoor aerosols demonstrating its applicability for apportionment of specific aerosol sources (Ott and Siegmann, 2006; Matter et al., 1999; Bukowiecki et al., 2002; Kittelson et al., 2005; Burtscher, 2005). However, to detect a strictly material-dependent chemical fingerprint, the aerosol must have a homogeneous surface material composition, both the PC and DC signal must be dominated by the aerosol material of interest, and the DC signal must scale with the same particle geometric and concentration parameters as the PC signal. Alternatively, in a heterogeneous aerosol mixture, samples with high concentrations of nuclei mode particles may be identified by using the PC to DC ratio (Bukowiecki et al., 2002). Corona-charged DC sensors yield signals approximately linear in both particle concentration (N) and particle diameter (d_p), $i \sim Nd_p^{1.1}$ (Marra et al., 2010; Jung and Kittelson, 2005; Fierz et al., 2011; Asbach et al., 2012) for particles with diameters between 20 and 200 nm. For polydisperse aerosols, the relation $i \sim N\bar{d}_m$ may be used where \bar{d}_m the first moment average (arithmetic mean) diameter of a mobility-equivalent diameter distribution (Nishida et al., 2019).

In the case of PC devices, however, the photoemission yield is considered proportional to photoelectrically active surface area (σ_{ph}) (Burtscher, 1992). The latter is defined only as the part of the surface which contributes to photoemission. In the free molecular regime, the inverse of particle mobility is largely proportional to the square of mobility diameter, d_m^2 . The dependence of photoemission yield on the inverse of particle mobility has been demonstrated in the free molecular and transition regimes ($20 < d_p < 100$ nm) for sintered spheres and fractal-like silver agglomerates (Schmidt-Ott et al., 1990; Schmidt-Ott, 1988; Zhou et al., 2013), recrystallized Ag and Au (Keller et al., 2001), poly-aromatic hydrocarbon (PAH) coated graphite aerosols (measured by diffusion battery) (Niessner, 1986), carbon agglomerates (Burtscher, 1992; Nishida et al., 2018), and diesel soot (Burtscher et al., 1998; Kittelson et al., 2005).

The photoemission quantum yield can be measured from the slope of total photoelectric yield as a function of photoelectrically active surface area (σ_{ph}). Quantum yields are found to be a strong function of material type, with relatively large values for silver, polycyclic aromatic hydrocarbons (PAHs) and elemental carbon, whereas aerosols such as NaCl (Jung and Kittelson, 2005), di-octyl sebacate (DOS), and secondary organic aerosols are weak photoemitters in the UV spectrum. Conversely, the presence of adsorbates such as water on photoemitting particles are found to reduce or eliminate photoemission (Zhiqiang et al., 2000; Bukowiecki et al., 2002).

The photoelectric quantum yield has also been found to vary between different morphologies of the same homogeneous material type. Three studies which discuss morphology effects on aerosol photoemission in detail seemingly contradict one another (Zhou et al., 2013; Keller et al., 2001; Schmidt-Ott, 1988). Zhou et al. (2013) found the overall charging efficiency of silver aggregates to be 0.4-0.8 times that of silver spheres of the same mobility diameter. This result disagrees with an existing photocharging theory which suggests that particles of the same material type and mobility should have the same photoelectric charging efficiency regardless of their morphology (Keller et al., 2001). Further, Schmidt-Ott (1988) demonstrated that sintering reduced the photoelectric charging efficiency of silver agglomerates, though the effects of changes in particle mobility and morphology were treated together as a function of sintering temperature. The author explained that the reduced photoelectric efficiency of the sintered particles was due to the reduced number of primary particles exposed to the surrounding gas molecules. Schmidt-Ott (1988) proposed photoelectric charging as an *in situ* measure of particle shape factors. The analysis suggests the charging efficiency of agglomerates should be higher than that of spheres with the same mobility diameter, but such results have not been directly compared.

Since direct UV photoelectric charging yield depends on material type and the charging rate depends on the photoelectrically active particle surface area, photoelectric charging could be valuable for source-apportionment studies and/or studies of exposure to specific, harmful aerosols within heterogeneous aerosol mixtures. Any practical measurement device or diagnostic technique must be accompanied by sufficient understanding and interpretation of measurements using validated particle photoemission theory.

In this work, a fixed-wavelength UV light source and detection system are used to measure photoemission from silver agglomerates and sintered spheres to determine the effects of particle size and morphology on photo-emission yield. Unconditioned soot particles from a propane

flame are measured to demonstrate the effect on photoemission of different particle material types when compared with silver agglomerates. The photoelectrically active area is evaluated to determine the effect of particle morphology on total photoelectric yield.

2 Theory

There are three steps involved in photoemission from surfaces in a vacuum (Spicer, 1967) and a fourth step is included for particles in a carrier gas (Burtscher, 1992):

1. absorption of a photon and excitation of an electron;
2. movement of the electron to the surface;
3. overcoming of the surface potential; and
4. removal of the electron from the vicinity of the particle.

After photoemission, the remaining particle develops a positively charged electrostatic field which reduces the probability of further release of electrons. Step 1 requires that the photoemitting material be exposed to the photon flux, and step 4 requires that photoemitting material be located externally-to the particle rather than shielded inside the same. Electrons emitted from the particle interior may be reabsorbed by material within the same particle and never escape the particle exterior (Weber et al., 1999).

The rate of photoemission for a particle, $\alpha^{q \rightarrow q+1}$, leading to particle charging from charge level q to $q + 1$, can be written as (Cardona and Ley, 1978; Maisels et al., 2002)

$$\alpha^{q \rightarrow q+1} = Y_q \frac{I}{4h\nu} \sigma_{\text{ph}} \quad (1)$$

where

$$Y_q = K_c (h\nu - \Phi^{q \rightarrow q+1})^m \quad (2)$$

in which I is the radiative energy flux, σ_{ph} is the photoelectrically active area, $h\nu$ is the specific photon energy, ν is the wavelength of light and h is Planck's constant (6.626068×10^{-34} kg m²s⁻¹). The non-dimensional quantum yield (Y_q) is a function of the charge state (q) and the proportionality constant (K_c). The latter is material dependent and empirically determined. Previous studies have determined an empirical exponent value (m) of approximately two for both metals and a few non-metals (Müller et al., 1988b; Schmidt-Ott and Federer, 1981; Jiang et al., 2007a).

The factor of 4 in the denominator of Eq. 1 represents the difference between the total surface area and cross-sectional area of a sphere, and is included here for consistency.

Photoemission occurs under conditions in which the specific photon energy is higher than the work function ($\Phi^{q \rightarrow q+1}$), which increases with each emitted charge due the resulting stronger electrostatic field until a maximum photoelectric charge state is reached. The charge-dependent work function ($\Phi^{q \rightarrow q+1}$) is a function of the particle electrical capacitance, or ability to hold charge, which is in turn a function of particle size and morphology (Cao et al., 2015). It has been demonstrated that the effect of the particle capacitance, along with differences in modelled or roughly estimated geometric surface area, account for a 17-30% increase in unipolar diffusion charging efficiency of agglomerates over spheres of the same material (Cao et al., 2015; Shin et al., 2010; Wang et al., 2010; Oh et al., 2004).

The electrons released via photoemission from particles in a carrier gas collide with neutral gas molecules, forming gaseous ions. It has been previously shown that under conditions where the recombination rate of ions with charged particles is not dominant, the total photoelectric activity generated over the total irradiation time (t_{irr}) can be measured by collecting the total current of photoemitted electrons (i_e), or the remaining positively charged particles (i_o) (Nishida et al., 2017, 2018). For polydispersed particle size distributions over a range of conditions, the contribution of each photoemission event to the net photoelectric current may be assumed to be independent (Nishida et al., 2019). The photoelectric current can be determined as follows

$$i = i_o = -i_e = cY A_{\text{ph}} \quad (3a)$$

$$c = \frac{I}{4h\nu} t_{\text{irr}} Q e \quad (3b)$$

$$A_{\text{ph}} = N \int_0^\infty p(d_p) \sigma_{\text{ph}}(d_p) dd_p \quad (3c)$$

where c is an operation constant which depends on the volumetric flow rate of the gas carrying the particles (Q), and the electron charge (e). The total photoelectrically active area (A_{ph}) is the integral sum of the photoelectrically active area (σ_{ph}) for the probability density function ($p(d_p)$) of particle diameter (d_p) multiplied by the total number concentration (N). For a monodisperse particle distribution, $A_{\text{ph}} = N\bar{\sigma}_{\text{ph}}$ where N is total number concentration. For the sufficiently large difference between the specific photon energy ($h\nu$) and the work functions (Φ) considered in this work, the quantum yield, Y , of Eq. 3 may be considered constant for a given material and morphology; an assumption which is valid for charge states sufficiently below the photoelectric charging limit (Maisels et al., 2002; Nishida et al., 2017).

The photoelectrically active area of a particle (σ_{ph}) accounts for the total area of material active in the process of photoemission; area which is exposed to the particle surroundings rather than shielded inside the particle. The sizes of particles under consideration are smaller than the wavelength of incident light such that absorption and electron excitation occurs throughout the whole particle volume (Schmidt-Ott, 1988; Burtscher, 1992; Müller et al., 1988a). For agglomerates, the primary particles' size is the relevant size for absorption (Dobbins et al., 1994)

and is estimated to be below 30 nm in each case of the current study following the methodology developed by Eggersdorfer et al. (2012). The diameters of sintered particles considered are below 60 nm, also well below the wavelength of incident light. The electrons must be excited sufficiently close to the surface of the particle to escape (Schmidt-Ott, 1988) and there is a higher likelihood of escape for electrons excited near the particle surface.

For monodisperse spheres of homogeneous material, assuming photoemission takes place over the whole particle surface area, $\sigma_{\text{ph}}(d_p) = \pi d_p^2 = \pi d_m^2$, which brings Eq. 3 in line with the photoemission equations as presented for modelling purposes (Maisels et al., 2002; Jiang et al., 2007a,b; Nishida et al., 2017). For a polydisperse size distribution of spheres, A_{ph} in Eq. 3c is equal to the area (A_m) defined here as the second moment of the mobility-equivalent diameter (d_m) distribution multiplied by the total number concentration and π ,

$$A_m = N \int_0^\infty p(d_m) \pi d_m^2 dd_m = \pi N d_{m,2}^2. \quad (4)$$

where $d_{m,2}$ is the second moment average diameter of the mobility distribution.

Mobility diameter and mobility size distributions can be easily measured and are widely utilized in aerosol science (Flagan, 1998). Mobility diameter has also been utilized by others to characterize aerosol surface area instruments. Jung and Kittelson (2005) measured the size and composition-dependent responses of two unipolar charging-based instruments and one photoelectric instrument as a function of Fuchs surface area, which is directly proportional to the particle mobility diameter and measurement regime. Therefore, the mobility diameter may be used in the photoelectric charging equations by neglecting the effect of particle morphology (Nishida et al., 2018). However, total photoelectric yield, as measured by electrical current in Eqn 3, is proportional to the photoelectrically active surface, which can be conflated with geometric surface area or an equivalent surface area based on mobility measurements. In the following sections, we test the hypothesis that the photoelectric current is proportional to the second moment of the mobility-equivalent diameter distribution: $i \sim N d_{m,2}^2$ for different particle morphologies and materials.

3 Experimental Method

The experimental method allowed measurements of photoelectric yield for a range of known concentrations, sizes, and morphologies of monodisperse, initially neutral particles. The experimental apparatus is shown in Fig. 1. The aerosol source was either carbonaceous soot or silver (Ag) particles. Carbonaceous soot particles were produced, as described in section 2.1 of Stettler et al. (2013), by burning propane (flow rate of 105 std cm³ min⁻¹) with air (1.2 std L min⁻¹) in a co-flow inverse diffusion flame using N₂ (3 std L min⁻¹) as a sheath flow, followed by ageing in an ageing chamber. A vacuum pump (Edwards, Burgess Hill, UK: Model Speedivac 2) and mass flow controller (Alicat Scientific, Tucson, AZ, USA) were used to draw

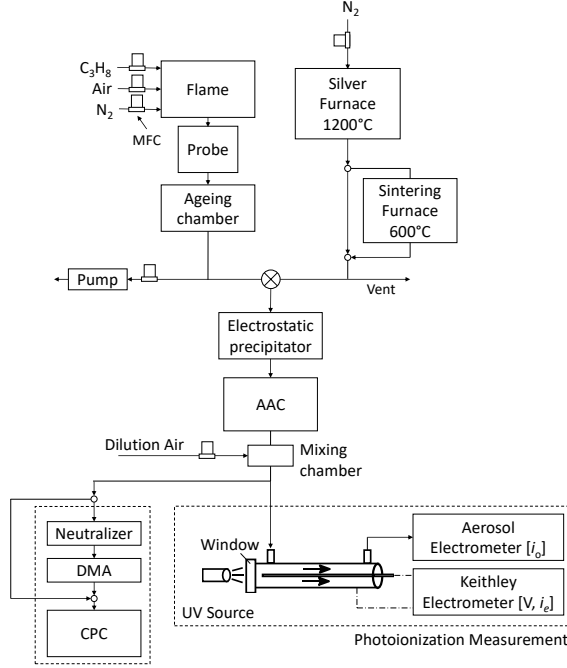


Figure 1: Schematic of experimental apparatus.

the sample flow through the ageing chamber at a constant flow rate of $1.5 \text{ std L min}^{-1}$. Silver agglomerate particles were produced by evaporation and subsequent condensation using a tube furnace operated at $1200^\circ C$ (Lenton, Hope, UK: Model LTF 12/25/500). Inside the furnace, a flow of HEPA-filtered, dry N_2 at 2 std L min^{-1} carried evaporated silver from three evenly distributed combustion boats containing pure silver. The aerosol sample flow either bypassed or passed through a second furnace (Elite Thermal Systems Ltd., Market Harborough, UK: Model THH12/90/305) operated at $600^\circ C$ to sinter the agglomerate particles into close-packed structures (Schmidt-Ott, 1988; Zhou et al., 2013).

The sample was drawn through an electrostatic precipitator operated at 8 kV from either aerosol source to capture particles with any residual charge from generation, as confirmed using an aerosol electrometer (TSI Inc., Shoreview, MN, USA: Model 3068B). The neutral particles were then passed through an Aerodynamic Aerosol Classifier (AAC; Cambustion Ltd., Cambridge, UK) which classifies particles based on aerodynamic diameter. The AAC selects particles of a given aerodynamic diameter by inducing a centrifugal force using rotating concentric cylinders, while controlling the particle residence time using a sheath flow. Only particles with the selected terminal velocity or particle relaxation time follow the correct trajectory to pass through the classifier. The AAC thus produces a monodisperse aerosol independent of the particle charge state, thereby providing relatively high concentrations of monodisperse, neutral particles¹ compared with particle classification via a Differential Mobility Analyzer (DMA) and subsequent charge conditioning (Johnson et al., 2018b).

To control the sample flow rate through the AAC and resulting dilution ratio, HEPA filtered air was added downstream of the AAC to balance the flows. Three dilution ratios (0.3, 1.65, and 4.4) were used for both aerosol sources to provide a range of particle concentrations at each classified size, which was determined by the AAC setpoint. A mixing chamber was used

¹when used in series with a electrostatic precipitator

to ensure the dilution air and sample flow were thoroughly mixed before entering the parallel measurement equipment.

The number-weighted particle mobility diameter distribution, allowing the particle Count Median Diameter (CMD) to be estimated, was measured with a Scanning Mobility Particle Sizer (SMPS; TSI Inc.: 3080 Electrostatic Classifier, Kr-85 Neutralizer, 3081 DMA, 3776 Condensation Particle Counter [CPC]) with two scans per AAC setpoint. Before and after the SMPS scans at each AAC setpoint, the neutralizer-DMA was bypassed and the total particle number concentration (N) was measured using the CPC.

In parallel to the SMPS, a portion of the aerosol sample was passed through a UV photoionization chamber and irradiated with UV light while simultaneously being exposed to a constant electric field between two concentric electrodes. A 3W UV lamp (Dinies Technologies GmbH, Germany: Model Mini3W-52ozon) provided ultraviolet light through a UV-extended fused silica optical window at wavelengths of 185 nm and 254 nm. A DC voltage in series with an amperometer was applied to the electrodes using a Keithley electrometer (Keithley Instruments Inc., Cleveland, OH, USA: Model 6517B). A constant applied voltage of 30 V (24 V cm^{-1}) was chosen to capture the highly mobile ions created from the photoemission process without significantly capturing the charged particles (Nishida et al., 2018, 2017). The electrometer measured the electrode current dominated by the photoemitted electrons (i_e) with a noise level less than ± 1 fA (Keithley Instruments, Inc., 2009). However, significant electrical noise from other sources increased the signal uncertainty and the results from the electrode current (i_e) were not included in this work. A flow rate of $1.5 \text{ std L min}^{-1}$ through the photoionization chamber was provided by the aerosol electrometer which measured the electrical current due to particle filtration in a Faraday cup electrometer (i_o) with a noise level lower than 1 fA at one second averaging time (TSI Inc., 2006a). Further specifications of the photoionization chamber and photoelectric current measurement may be found in Nishida et al. (2018).

Throughout the experimental set-up, stainless steel and conductive silicon tubing were used to minimize particle electrostatic losses in the sampling lines. System flow rates were verified using a bubble flow meter (Gilibrator 2, Sensidyne, LP, Clearwater, FL, USA).

3.1 Measurement uncertainty

Uncertainty in aerodynamic diameter for an AAC set-point was considered to be 4.7% based on the maximum average disagreement for spherical particles (Johnson et al., 2018a). Uncertainty of the count median (mobility) diameter (CMD) from the SMPS was considered to be 3% (Kinney et al., 1991). Concentrations were measured using the CPC with an uncertainty of 10% (TSI Inc., 2006b). For data points where the direct CPC measurement was in photometric mode, the number concentration from the SMPS was used with an uncertainty of 10%, consistent with published values (Wiedensohler et al., 2012). Vertical error bars were not included in the figures as the standard error in i_o current measurements were less than 1.5% for all but two data points using 30 s averages of measurements collected at 1 Hz.

3.2 Particle characterization

The particle aerodynamic diameter (d_{ae}) classified by the AAC in tandem with the mobility diameter (d_m) classified by the downstream DMA provided the ability to determine several particle geometrical parameters by assuming the bulk density of the particle material, and that the mobility and aerodynamic measurements were collected in approximately the same gas conditions. Average volume equivalent diameter, $d_{ve} = f(d_{ae}, d_m)$ (Tavakoli et al., 2014), effective density, $\rho_{eff} = f(d_{ae}, d_m)$, and particle mass, $m = f(\rho_{eff}, d_m)$ (McMurry et al., 2002) were estimated. The bulk density of silver of $\rho = 10.5 \times 10^3 \text{ kg m}^{-3}$ was used for the calculation of d_{ve} for silver agglomerates. The relationship between particle mobility and effective density was measured and described using the mass-mobility exponent, D_{fm} , and pre-factor, k_m (DeCarlo et al., 2004).

While the AAC generates an aerosol source that is monodispersed in aerodynamic diameter (Tavakoli et al., 2014), the range of equivalent mobility diameters of the classified particles depends on their effective density (DeCarlo et al., 2004). Spherical particles with a constant effective density that are monodispersed in aerodynamic diameter are also monodispersed in mobility. However, particles are often agglomerates, which results in their effective density decreasing with increasing particle mobility diameter (Olfert and Rogak, 2019). For example, a small particle with low drag and mass, and a large particle with high drag and mass will have the same aerodynamic diameter, but different mobility diameters. The AAC classified particles being broader in mobility diameter due to their morphology (i.e. changing effective density with size) was quantified by the downstream SMPS measurements. The geometric standard deviation (GSD) of the mobility size distribution of the AAC classified particles varied from 1.20 to 1.30 for the sintered silver, 1.28 to 1.35 for the silver agglomerates, and 1.18 to 1.35 and 1.53 to 1.59 for the unconditioned soot at small ($<140 \text{ nm}$) and large ($>140 \text{ nm}$) mobility CMDs, respectively. These GSDs are broader than their aerodynamic GSD (<1.1) (Johnson et al., 2018b), and agree with the physical understanding that as particles become less spherical and larger, the range of mobility diameters at the same aerodynamic diameter becomes wider.

To verify the effects of sintering on particle morphology, samples of raw and sintered silver particles were mobility size selected with a DMA and deposited on a silicon substrate using an electrostatic precipitator. Scanning electron microscope (SEM: LEO GEMINI 1530VP FEG-SEM) images were captured under a 10 kV acceleration voltage and are shown in Fig. 2. Figure 2a shows that the sintered silver particles captured at $d_m = 40 \text{ nm}$ are largely sintered into spheres. Figure 2b shows sintered silver particles with mobility diameter $d_m = 85 \text{ nm}$ approximate close-packed spheres and have a significantly different morphology from the raw agglomerate silver particles at the same mobility size shown in Fig. 2c. The mass-mobility exponent (D_{fm}) and prefactor (k_m) were calculated from the tandem AAC-DMA measurements (Tavakoli and Olfert, 2014) for silver agglomerates ($D_{fm} = 2.49, k_m = 0.72$) and close-packed spheres ($D_{fm} = 2.78, k_m = 153$), respectively, further demonstrating that the particles changed morphology due to sintering (DeCarlo et al., 2004).

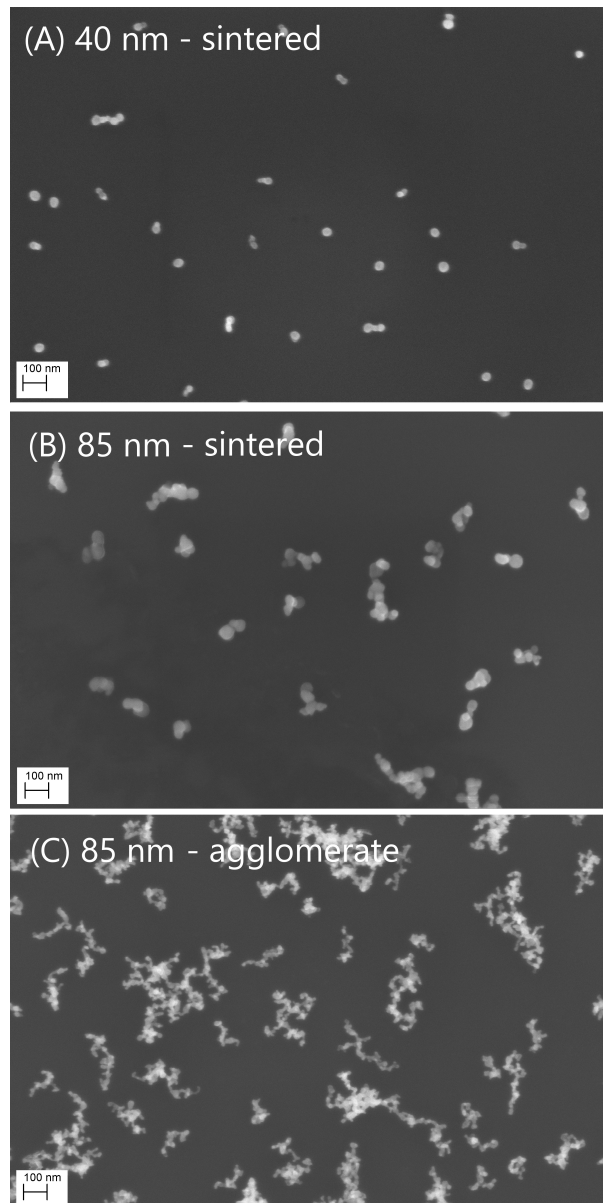


Figure 2: SEM images of mobility selected silver nanoparticles: (A) sintered spheres, $d_m = 40$ nm, (B) sintered, close-packed spheres, $d_m = 85$ nm, (C) raw agglomerates, $d_m = 85$ nm.

4 Results

4.1 Photoelectric yield as a function of particle size, concentration, and material

The electrical currents resulting from photoemission from aerodynamically monodisperse, silver and soot agglomerates were measured across a range of particle mobility CMDs (Ag, 20-110 nm, Soot, 40-200 nm), and total number concentrations (Ag, $1.8 \times 10^4 - 3.8 \times 10^6 \text{ cm}^{-3}$, Soot, $3.3 \times 10^4 - 8 \times 10^5 \text{ cm}^{-3}$). The high coefficient of determination demonstrates that number concentration and particle mobility are suitable measurements for comparison. Using a similar evaluation methodology, other available particle parameters such as aerodynamic diameter and mass were not suitable. The near linearity with number concentration demonstrates that photoelectric measurements may be investigated on a per particle basis. Electrical currents resulting from photoemission (i_o) are shown on a per particle basis as a function of mobility CMD measured by the SMPS in parallel in Figure 3. The current normalized by number concentration (i_o/N) corresponds to a mean charge per particle when divided by volumetric flow rate (Q) and electron charge (e), *i.e.* charge per particle = $i_o/(NQe)$. A linear regression fit yields $i_o \sim Nd_m^2$ for silver agglomerates and $i_o \sim Nd_m^{1.95}$ for soot particles, with coefficients of determination of 0.99 and 0.93, respectively, where d_m is taken to be particle mobility CMD. Both fit exponents are approximately 2, thereby confirming that the second moment of the mobility size distribution of both spherical and non-spherical particles is a suitable measurement for comparison as described in Eq. 4.

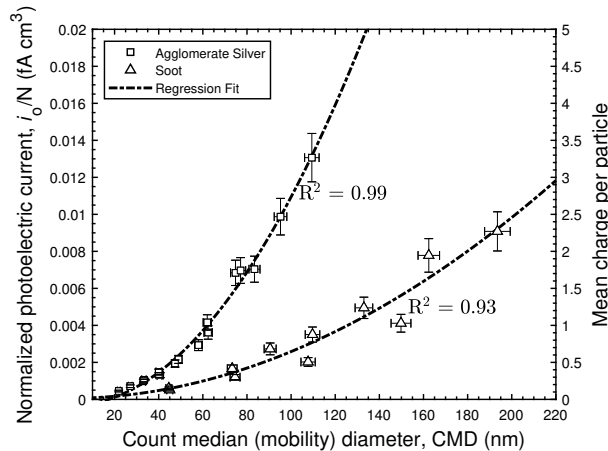


Figure 3: Photoelectric current normalized by number concentration (i_o/N) as a function of particle count median diameter (CMD) using a 30 V (24 V/cm) ion capture voltage for silver agglomerates. A regression fit yields $i_o \sim Nd_m^2$ for silver and $i_o \sim Nd_m^{1.95}$ for soot, with coefficients of determination of 0.99 and 0.93, respectively.

Figure 4 shows the photoelectric current as a function of A_m defined in Eq. 4 as proportional to the second moment of the mobility diameter distribution. Agglomerate silver shows a photoelectric yield approximately five times higher than the propane flame soot when based on the same calculation of A_m . Carbon has a higher work function than silver (for soot, ≈ 4.95 eV, Ag, 4.25-4.75 eV (Michaelson, 1977)). Calculating the expected enhancement due the difference in work functions of soot and silver agglomerates (4.95 eV and 4.33 eV for soot (Michaelson, 1977) and Ag (Zhou and Zachariah, 2012), respectively), using Eq. 2 with a constant value for K_c , results in an expected enhanced yield of approximately 1.8 times. The five times enhance-

ment in photoelectric yield of silver agglomerates over soot agglomerates is not fully explained by the difference in the work functions, and a further material or surface dependency must be considered.

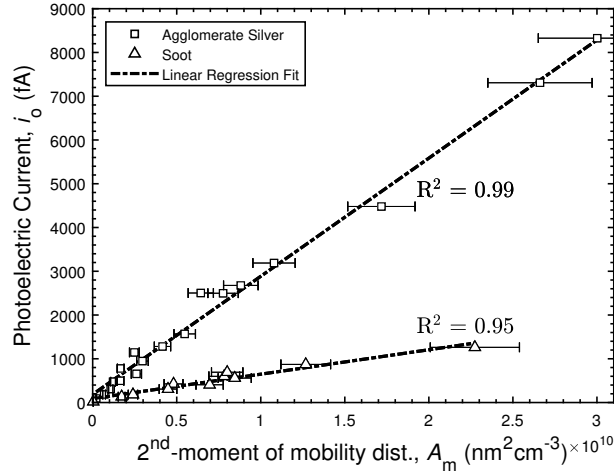


Figure 4: Photoelectric current, i_o , as a function of $A_m = \pi N d_{m,2}^2$ (Eqn. 4), defined as proportional to the second moment of a mobility diameter distribution, for agglomerate silver and unconditioned soot from a propane flame. Coefficients of determination for agglomerate silver and unconditioned soot are 0.99 and 0.95, respectively.

4.2 Effects of particle morphology on photoelectric yield

Figure 5a shows that the measured photoelectric current (i_o) is an approximately linear function of A_m as defined in Eq. 4 for both agglomerate and sintered silver particles. For $A_m < 1.2 \times 10^{10} \text{ nm}^2 \text{ cm}^{-3}$, linear coefficients of determination for silver agglomerates and spheres are 0.96 and 0.98, respectively. The corresponding slopes of the curves indicate that agglomerate silver has a photoelectric yield approximately 2.6 times higher than sintered silver when normalized by A_m . This result contradicts previous research which suggests silver agglomerates have a lower photoelectric yield than sintered silver particles of the same mobility diameter (Zhou et al., 2013), or that the photoelectric yield for particles of the same material and mobility diameter should be the same regardless of their morphology (Keller et al., 2001). However, the findings of the current study agree with Schmidt-Ott (1988) which found agglomerate silver offers more material exposed to the particle surroundings compared with a close-packed structure of the same mobility size that results from particle sintering (Schmidt-Ott, 1988). In a close-packed structure, more constituent material is shielded inside the particle such that some photoemitted electrons may be reabsorbed by material within the same particle never to escape the particle exterior (Weber et al., 1999). A factor of 2.6 increase in photoelectric current from agglomerates over spheres of the same material type and mobility diameter is significantly higher than the 17-30% demonstrated by unipolar diffusion charging (Cao et al., 2015; Shin et al., 2010; Wang et al., 2010; Oh et al., 2004). With measurements of particle concentration, mobility diameter, and photoelectric yield, the active area multiplier of photoelectric yield may be calculated, thereby giving a measure of the state of sintering.

Figure 5b shows photoelectric current (i_o) as a function of a photoelectrically active area ($A_{ph} = \pi N d_{cl}^{3S}$) using a shape factor (S) defined in Schmidt-Ott (1988) and Appendix A

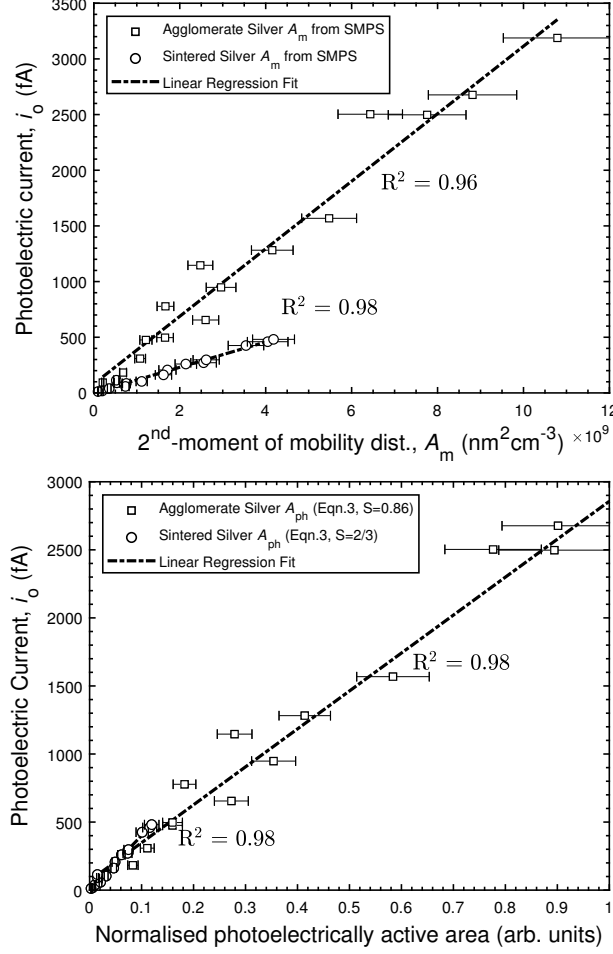


Figure 5: Photoelectric current as a function of (A) $A_m = \pi N d_{m,2}^2$ (Eqn. 4), defined as proportional to the second moment of a mobility diameter distribution, and (B) photoelectrically active area ($A_{ph} = \pi N d_{cl}^{3S}$) derived from Eqn. A-3 (Schmidt-Ott, 1988).

(Eq. A-3). The shape factor, $S = 2/3$, was selected for the sintered silver particles based on the close-packed particle morphology identified by the SEM images (*i.e.* $d_{cl} = d_m$). For the agglomerate silver particles, it was assumed that the volume equivalent diameter (d_{ve}) represents the diameter of the equivalent close-packed particle of Eq. A-3, *i.e.* $d_{cl} = d_{ve}$. The silver agglomerate shape factor (S) of 0.86 was determined based on regression using the coefficient of determination and is comparable to previous values of $S = 0.92$ and $S = 0.74$, for diffusion grown agglomerates determined by experiments and simulation, respectively (Schmidt-Ott, 1988; Meakin and Witten Jr, 1983). This result also agrees with our physical understanding that shape factor increases as the particle radius of gyration increases as discussed in Appendix A. This fitting parameter (S) is affected by, but does not explicitly consider, the area of particles exposed to the particle surroundings. The photoelectrically active area calculated using the fitting parameter (S) requires arbitrary units which makes physical interpretation difficult.

The amount of particle material exposed to its surroundings may not fully account for the factor of 2.6 difference in photoelectric yield for silver agglomerates compared with sintered spheres for the same A_m and material. The effect of morphology on particle electrical capacitance (Cao et al., 2015) has some small, but significant effect limited conservatively to 30% (Cao et al., 2015; Shin et al., 2010; Wang et al., 2010; Oh et al., 2004). Furthermore, some oxidation or

other changes in surface properties might have occurred during either the particle formation or sintering processes, which could affect the particle work function or proportionality constant (K_c) even though both processes take place in the same N_2 environment. Similarly, changes in the material structure at the atomic level could have occurred during sintering which might affect K_c . Zhou and Zachariah (2012) measured small changes in work function after sintering of silver particles conservatively between 4.25 eV and 4.35 eV, with values for agglomerates showing a slightly higher work function than spheres. This change in work function could explain up to a 10% change in photoelectric yield, though favoring spheres to have higher photoelectric yield than agglomerates. Electrons excited internally in a particle are less likely to escape than those excited near the surface (Schmidt-Ott et al., 1980). For that reason, electrons are more likely to escape particles of the same mass as the particle radius of gyration increases. This provides a qualitative explanation for a higher quantum yield for aerosols with smaller primary particles. The depth through which electrons must travel within a primary particle to escape is not considered explicitly in this work. Further work is required to determine the fundamental definition of photoelectrically active area, which may be related to geometric surface area or other particle properties.

5 Conclusions

Photoelectric currents were measured to determine the effects of particle size, concentration, material and morphology on photo-emission yield using a fixed-wavelength UV light source. An aerodynamic aerosol classifier was used in series with an electrostatic precipitator to select neutral, monodispersed agglomerate or sintered silver particle to determine the photoelectric yield from particles of the same material and different morphologies. Unconditioned soot particles from a propane flame are measured to demonstrate the effect of different particle material types when compared with silver agglomerates. Each of the measured photoelectric currents was shown to be linearly proportional to the second moment of the particle mobility size distribution for a range of particle sizes and concentrations of self-similar particle material type and morphologies. Photoelectric yields of agglomerate silver particles were shown to be $5\times$ higher photoelectric yield than soot from a propane flame. In this work, it is shown that agglomerate silver particles offer a significantly higher photoelectric yield ($2.6\times$) than sintered, close-packed spheres of the same material and equivalent mobility size, directly contradicting two of the most recent previous studies which discuss the subject in detail.

A sintered, close-packed sphere has less active surface area of material located adjacent to the particle surrounding, compared to an agglomerate of the same particle mobility diameter. The mechanisms of photoemission include electron removal from the vicinity of the particle, which occurs for photoemitting material exposed to the particle surroundings rather than for material shielded inside each particle. Therefore, the photoelectrically active area must account for the effect of particle morphology and cannot be assumed to be the same as that of a mobility-equivalent sphere. Finally, the observed morphology dependency of aerosol photoelectric current measurements may enable measurements of the particle active surface area and therefore the state of sintering when the particle mobility size and concentration are known.

Acknowledgments

The authors gratefully acknowledge Alphasense Ltd., Cambridge Trust, and the Natural Sciences and Engineering Research Council of Canada (NSERC) for financial support. The authors thank Cambustion Ltd. for providing the AAC and Xiao Zhang for capturing the SEM images.

A Exposed surface shape factor

Schmidt-Ott (1988) introduced an *in situ* method for measurement of particle shape factors by comparing mobility and photoelectric activity of particles in a carrier gas before and after sintering silver agglomerates into close-packed spheres. The author defined a shape factor (S) which accounts for the proportion of primary particles exposed to the gas surrounding the agglomerate, and quantified S using measurements of photoelectric activity. The method for relating the exposed surface to photoelectric activity is presented and applied here to provide context for the analysis of photoelectrically active area.

For structures grown by diffusion-limited aggregation, the number of primary particles exposed to the surrounding gas molecules ($n_{pp,e}$) is assumed to be proportional to the total number of primary particles (n_{pp}) raised to a power (S)

$$n_{pp,e} \sim n_{pp}^S \quad (\text{A-1})$$

where S is defined as a shape factor. Only primary particles exposed to the surrounding gas experience collisions with gas molecules, thus acting as a shield for the interior primary particles.

The total number of primary particles (n_{pp}) in a close-packed sphere of diameter (d_{cl}) is given by

$$n_{pp} \sim d_{cl}^3 \quad (\text{A-2})$$

where d_{pp} is primary particle diameter and the ratio of d_{cl}/d_{pp} is large.

Following Schmidt-Ott (1988), by combining Eqs. A-1 and A-2, and assuming that the photoelectric activity is linearly proportional to the number of exposed primary particles ($n_{pp,e}$),

the photoelectric activity, ε (defined as the number of electrons emitted from an agglomerate particle), is proportional to the number of particles exposed to the surroundings, and therefore its equivalent close-packed sphere diameter after sintering (d_{cl}) raised to a power $3S$, according to:

$$\varepsilon \sim d_{cl}^{3S} \quad (\text{A-3})$$

The case where all of the primary particles are exposed in an idealized straight-chain morphology leads to a shape factor limit S near unity. Conversely, the highest shielding configuration of primary particles occurs for a close-packed sphere, where S approaches $2/3$ for a large ratio of d_{cl}/d_{pp} . A value of $S = 0.92$ was found for silver agglomerates generated with an evaporation/condensation process (Schmidt-Ott, 1988).

Bibliography

- Asbach, C., Kaminski, H., Von Barany, D., Kuhlbusch, T. A. J., Monz, C., Dziurawitz, N., Pelzer, J., Vossen, K., Berlin, K., Dietrich, S., et al. (2012). Comparability of portable nanoparticle exposure monitors. *Annals of occupational hygiene*, 56(5):606–621.
- Bukowiecki, N., Kittelson, D. B., Watts, W. F., Burtscher, H., Weingartner, E., and Baltensperger, U. (2002). Real-time characterization of ultrafine and accumulation mode particles in ambient combustion aerosols. *Journal of Aerosol Science*, 33(8):1139–1154.
- Burtscher, H. (1992). Measurement and characteristics of combustion aerosols with special consideration of photoelectric charging and charging by flame ions. *Journal of Aerosol Science*, 23(6):549–595.
- Burtscher, H. (2005). Physical characterization of particulate emissions from diesel engines: a review. *Journal of Aerosol Science*, 36(7):896–932.
- Burtscher, H., Künzel, S., and Hüglin, C. (1998). Characterization of particles in combustion engine exhaust. *Journal of Aerosol Science*, 29(4):389–396.
- Burtscher, H., Scherrer, L., Siegmann, H. C., Schmidt-Ott, A., and Federer, B. (1982). Probing aerosols by photoelectric charging. *Journal of Applied Physics*, 53(5):3787–3791.
- Burtscher, H., Schmidt-Ott, A., and Siegmann, H. C. (1984). Photoelectron yield of small silver

- and gold particles suspended in gas up to a photon energy of 10 eV. *Zeitschrift für Physik B Condensed Matter*, 56(3):197–199.
- Byeon, J. H. and Roberts, J. T. (2014). Photoionization of nanosized aerosol gold agglomerates and their deposition to form nanoscale islands on substrates. *Langmuir*, 30(29):8770–8775.
- Cao, L. N. Y., Wang, J., Fissan, H., Pratsinis, S. E., Eggersdorfer, M. L., and Pui, D. Y. (2015). The capacitance and charge of agglomerated nanoparticles during sintering. *Journal of Aerosol Science*, 83:1–11.
- Cardona, M. and Ley, L. (1978). *Photoemission in solids I*. Springer-Verlag.
- DeCarlo, P. F., Slowik, J. G., Worsnop, D. R., Davidovits, P., and Jimenez, J. L. (2004). Particle morphology and density characterization by combined mobility and aerodynamic diameter measurements. Part 1: Theory. *Aerosol Science and Technology*, 38(12):1185–1205.
- Dobbins, R. A., Mulholland, G. W., and Bryner, N. P. (1994). Comparison of a fractal smoke optics model with light extinction measurements. *Atmospheric Environment*, 28(5):889–897.
- Eggersdorfer, M. L., Kadau, D., Herrmann, H. J., and Pratsinis, S. E. (2012). Aggregate morphology evolution by sintering: number and diameter of primary particles. *Journal of aerosol science*, 46:7–19.
- Fierz, M., Houle, C., Steigmeier, P., and Burtscher, H. (2011). Design, calibration, and field performance of a miniature diffusion size classifier. *Aerosol Science and Technology*, 45(1):1–10.
- Flagan, R. C. (1998). History of electrical aerosol measurements. *Aerosol Science and Technology*, 28(4):301–380.
- Hogan, C. J., Lee, M.-H., and Biswas, P. (2004). Capture of viral particles in soft X-ray-enhanced corona systems: charge distribution and transport characteristics. *Aerosol Science and Technology*, 38(5):475–486.
- Hontañón, E. and Kruis, F. E. (2008). Single charging of nanoparticles by uv photoionization at high flow rates. *Aerosol Science and Technology*, 42(4):310–323.
- Jiang, J., Hogan Jr, C. J., Chen, D.-R., and Biswas, P. (2007a). Aerosol charging and capture in the nanoparticle size range (6–15 nm) by direct photoionization and diffusion mechanisms. *Journal of Applied Physics*, 102(3):034904.

- Jiang, J., Lee, M.-H., and Biswas, P. (2007b). Model for nanoparticle charging by diffusion, direct photoionization, and thermionization mechanisms. *Journal of electrostatics*, 65(4):209–220.
- Johnson, T., Nishida, R., Irwin, M., Symonds, J., S. Olfert, J., and Boies, A. (2018a). Agreement Between Different Aerosol Classifiers Using Spherical Particles. In *Cambridge Particle Meeting*, Cambridge, UK. June 15, 2018.
- Johnson, T. J., Irwin, M., Symonds, J. P., Olfert, J. S., and Boies, A. M. (2018b). Measuring aerosol size distributions with the aerodynamic aerosol classifier. *Aerosol Science and Technology*, 52(6):655–665.
- Jung, H. and Kittelson, D. B. (2005). Characterization of aerosol surface instruments in transition regime. *Aerosol Science and Technology*, 39(9):902–911.
- Jung, T., Burtscher, H., and Schmidt-Ott, A. (1988). Multiple charging of ultrafine aerosol particles by aerosol photoemission (ape). *Journal of Aerosol Science*, 19(4):485–490.
- Keithley Instruments, Inc. (2009). *Model 6517B Reference Manual, Revision B*.
- Keller, A., Fierz, M., Siegmann, K., Siegmann, H. C., and Filippov, A. (2001). Surface science with nanosized particles in a carrier gas. *Journal of Vacuum Science & Technology A: Vacuum, Surfaces, and Films*, 19(1):1–8.
- Kinney, P. D., Pui, D. Y. H., Mullholland, G. W., and Bryner, N. P. (1991). Use of the electrostatic classification method to size 0.1 μm srm particles—a feasibility study. *Journal of Research of the National Institute of Standards and Technology*, 96(2):147.
- Kittelson, D., Watts, W., Savstrom, J., and Johnson, J. (2005). Influence of a catalytic stripper on the response of real time aerosol instruments to diesel exhaust aerosol. *Journal of Aerosol Science*, 36(9):1089–1107.
- Kulkarni, P., Namiki, N., Otani, Y., and Biswas, P. (2002). Charging of particles in unipolar coronas irradiated by in-situ soft X-rays: enhancement of capture efficiency of ultrafine particles. *Journal of Aerosol Science*, 33(9):1279–1296.
- Li, L. and Chen, D.-R. (2011). Aerosol charging using pen-type UV lamps. *Aerosol and Air Quality Research*, 11(7):791–801.
- Maisels, A., Jordan, F., and Fissan, H. (2002). Dynamics of the aerosol particle photocharging

- process. *Journal of Applied Physics*, 91(5):3377–3383.
- Marra, J., Voetz, M., and Kiesling, H.-J. (2010). Monitor for detecting and assessing exposure to airborne nanoparticles. *Journal of Nanoparticle Research*, 12(1):21–37.
- Matter, D., Mohr, M., Fendel, W., Schmidt-Ott, A., and Burtscher, H. (1995). Multiple wavelength aerosol photoemission by excimer lamps. *Journal of Aerosol Science*, 26(7):1101–1115.
- Matter, U., Siegmann, H. C., and Burtscher, H. (1999). Dynamic field measurements of submicron particles from diesel engines. *Environmental science & technology*, 33(11):1946–1952.
- McMurry, P. H., Wang, X., Park, K., and Ehara, K. (2002). The relationship between mass and mobility for atmospheric particles: A new technique for measuring particle density. *Aerosol Science & Technology*, 36(2):227–238.
- Meakin, P. and Witten Jr, T. A. (1983). Growing interface in diffusion-limited aggregation. *Physical Review A*, 28(5):2985.
- Michaelson, H. B. (1977). The work function of the elements and its periodicity. *Journal of Applied Physics*, 48(11):4729–4733.
- Mohr, M., Matter, D., and Burtscher, H. (1996). Efficient multiple charging of diesel particles by photoemission. *Aerosol Science and Technology*, 24(1):14–20.
- Müller, U., Burtscher, H., and Schmidt-Ott, A. (1988a). Photoemission from small metal spheres: A model calculation using an enhanced three-step model. *Physical Review B*, 38(11):7814.
- Müller, U., Schmidt-Ott, A., and Burtscher, H. (1988b). Photoelectric quantum yield of free silver particles near threshold. *Zeitschrift für Physik B Condensed Matter*, 73(1):103–106.
- Niessner, R. (1986). The chemical response of the photo-electric aerosol sensor (pas) to different aerosol systems. *Journal of Aerosol Science*, 17(4):705–714.
- Nishida, R., Yamasaki, N., Schrieffl, M., Boies, A., and Hochgreb, S. (2019). Modelling the effect of aerosol polydispersity on unipolar charging and measurement in low-cost sensors. *Journal of Aerosol Science*.
- Nishida, R. T., Boies, A. M., and Hochgreb, S. (2017). Modelling of direct ultraviolet pho-

- toionization and charge recombination of aerosol nanoparticles in continuous flow. *Journal of Applied Physics*, 121(2):023104.
- Nishida, R. T., Boies, A. M., and Hochgreb, S. (2018). Measuring ultrafine aerosols by direct photoionization and charge capture in continuous flow. *Aerosol Science and Technology*, 52(5):546–556.
- Oh, H., Park, H., and Kim, S. (2004). Effects of particle shape on the unipolar diffusion charging of nonspherical particles. *Aerosol Science and Technology*, 38(11):1045–1053.
- Olfert, J. and Rogak, S. (2019). Universal relations between soot effective density and primary particle size for common combustion sources. *Aerosol Science and Technology*, 53(5):485–492.
- Ott, W. R. and Siegmann, H. C. (2006). Using multiple continuous fine particle monitors to characterize tobacco, incense, candle, cooking, wood burning, and vehicular sources in indoor, outdoor, and in-transit settings. *Atmospheric Environment*, 40(5):821–843.
- Röhrbein, J. and Weber, A. P. (2018). A system for on-line characterization of gas-borne particle surface properties based on their photoemission. *Journal of Aerosol Science*.
- Schmidt-Ott, A. (1988). New approaches to in situ characterization of ultrafine agglomerates. *Journal of Aerosol Science*, 19(5):553–563.
- Schmidt-Ott, A., Baltensperger, U., Gäggeler, H. W., and Jost, D. T. (1990). Scaling behaviour of physical parameters describing agglomerates. *Journal of Aerosol Science*, 21(6):711–717.
- Schmidt-Ott, A. and Federer, B. (1981). Photoelectron emission from small particles suspended in a gas. *Surface Science*, 106(1-3):538–543.
- Schmidt-Ott, A., Schurtenberger, P., and Siegmann, H. C. (1980). Enormous yield of photoelectrons from small particles. *Physical Review Letters*, 45(15):1284.
- Shin, W. G., Wang, J., Mertler, M., Sachweh, B., Fissan, H., and Pui, D. Y. H. (2010). The effect of particle morphology on unipolar diffusion charging of nanoparticle agglomerates in the transition regime. *Journal of Aerosol Science*, 41(11):975–986.
- Spicer, W. E. (1967). Possible non-one-electron effects in the fundamental optical excitation spectra of certain crystalline solids and their effect on photoemission. *Physical Review*, 154(2):385.

- Stettler, M. E. J., Swanson, J. J., Barrett, S. R. H., and Boies, A. M. (2013). Updated correlation between aircraft smoke number and black carbon concentration. *Aerosol Science and Technology*, 47(11):1205–1214.
- Tavakoli, F. and Olfert, J. S. (2014). Determination of particle mass, effective density, mass-mobility exponent, and dynamic shape factor using an aerodynamic aerosol classifier and a differential mobility analyzer in tandem. *Journal of Aerosol Science*, 75:35–42.
- Tavakoli, F., Symonds, J. P. R., and Olfert, J. S. (2014). Generation of a monodisperse size-classified aerosol independent of particle charge. *Aerosol Science and Technology*, 48(3):i–iv.
- TSI Inc. (2006a). *Model 3068B Aerosol Electrometer, User’s Manual, Revision A*.
- TSI Inc. (2006b). *Model 3776 Ultrafine Condensation Particle Counter: Operation and Service Manual, Revision B*.
- Wang, J., Shin, W. G., Mertler, M., Sachweh, B., Fissan, H., and Pui, D. Y. H. (2010). Measurement of nanoparticle agglomerates by combined measurement of electrical mobility and unipolar charging properties. *Aerosol Science and Technology*, 44(2):97–108.
- Weber, A. P., Seipenbusch, M., and Kasper, G. (2001). Application of aerosol techniques to study the catalytic formation of methane on gasborne nickel nanoparticles. *The Journal of Physical Chemistry A*, 105(39):8958–8963.
- Weber, A. P., Seipenbusch, M., Thanner, C., and Kasper, G. (1999). Aerosol catalysis on nickel nanoparticles. *Journal of Nanoparticle Research*, 1(2):253–265.
- Wiedensohler, A., Birmili, W., Nowak, A., Sonntag, A., Weinhold, K., Merkel, M., Wehner, B., Tuch, T., Pfeifer, S., Fiebig, M., et al. (2012). Mobility particle size spectrometers: harmonization of technical standards and data structure to facilitate high quality long-term observations of atmospheric particle number size distributions. *Atmospheric Measurement Techniques*, 5:657–685.
- Zhiqiang, Q., Siegmann, K., Keller, A., Matter, U., Scherrer, L., and Siegmann, H. C. (2000). Nanoparticle air pollution in major cities and its origin. *Atmospheric Environment*, 34(3):443–451.
- Zhou, L., You, R., Tan, J., and Zachariah, M. R. (2013). Wavelength-resolved uv photoelectric charging dynamics of nanoparticles: comparison of spheres and aggregates. *Aerosol Science and Technology*, 47(6):672–680.

Zhou, L. and Zachariah, M. R. (2012). Size resolved particle work function measurement of free nanoparticles: Aggregates vs. spheres. *Chemical Physics Letters*, 525:77–81.